Polarization Effects in the AgBr Interaction Potential

Ching-Hwa Kiang† and William A. Goddard III*

Materials and Process Simulation Center, Beckman Institute (139-74), Division of Chemistry and Chemical Engineering,[‡] California Institute of Technology, Pasadena, California 91125

Received: April 13, 1995; In Final Form: July 28, 1995[∞]

A pairwise additive interaction potential (including a shell model to account for ion polarizabilities) was developed for describing crystalline AgBr. It was constructed by fitting experimental data, including lattice constant, phonon frequencies at the Γ and X points, dielectric constant, cohesive energy, and elastic constants. The predicted results compare favorably with experimentally measured values. The influence of polarization effects on the various crystal properties is discussed.

I. Introduction

Silver halides have long been the subject of experimental and theoretical study.¹ Interest in the photographic processes and in the ionic transport properties of silver halides has prompted much discussion about the crystal dynamics of these systems. In particular, the anomalous physical properties of AgBr and AgCl have been investigated extensively. The unusual electronic energy bands,² peculiar lattice dynamics,³,⁴ and exceptionally high mobility of the interstitial silver ions⁵,6 make these crystalline systems distinct from other isostructural alkali halides.¹ Practical theoretical study on AgBr and AgCl requires construction of an interionic potential model that can describe the uncommon behavior of silver halides. The development of a force field adequate to successfully represent the crystal potentials is essential if simulations are to lead to an understanding of the peculiar properties of silver halides.8

The first interaction potentials of silver halides were proposed by Mayer.⁹ This potential characterizes the system with strong short-range repulsion and long-range Coulomb and van der Waals attractions (dispersion). Recent attempts at constructing accurate interaction potentials of silver halides^{10,11} have used pairwise interactions (electrostatic, van der Waals attractions, and short-range repulsions) as well as some three-body terms. The undetermined coefficients in the potentials are fit to reproduce experimentally measured properties, such as lattice constant, cohesive energy, phonon dispersion curves, dielectric constants, and elastic constants. While some properties (elastic constant, dielectric constant, and cohesive energy) calculated from the potentials agree with experiment, the theoretically calculated phonon dispersion curves still do not agree satisfactorily with experiment.

An accurate potential for AgBr is essential for simulating the static as well as dynamic crystal properties; hence, we developed a new interaction potential simple enough for classical atomic simulations but accurate enough for phonon dispersion. This potential includes polarization effects via the classical shell model (CSM).^{3,12} This force field accounts for many of the experimental properties observed, such as the dielectric constant and phonon dispersion curves.

II. Method

We require the potential to be pairwise with a long-range Coulomb potential, a short-range interaction potential, and an energy due to the polarization of the particles in the crystal.

$$U = U_{\text{Coulomb}} + U_{\text{short}} + U_{\text{polar}} \tag{1}$$

All calculations use periodic boundary conditions.

The Coulomb potential is the dominant interaction in ionic crystals. The long-range Coulomb interaction between two ions is

$$U_{\text{Coulomb}} = C_{\text{Q}} \sum_{i,j} \frac{q_i q_j}{R_{ii}}$$
 (2)

where q_i and q_j are charges of the ions, cores, and shells in electron charge units, R_{ij} is the distance in angstroms between positions i and j, and $C_Q = 332.0637$ ensures that energies are in kcal/mol. The electrostatic interaction between a core and shell connected by a spring is excluded when using the shell model. The prime indicates exclusion of the i = j term and the core—shell terms.

The short-range potential function contains an attractive term of the London dispersion type $(1/R^6)$ as well as a repulsive term due to the Pauli exclusion principle. We adopt either the two-parameter Lennard-Jones potential

$$U_{\rm LJ} = D_0 \left\{ \left(\frac{R_0}{R} \right)^{12} - 2 \left(\frac{R_0}{R} \right)^6 \right\}$$
 (3)

or the three-parameter exponential-6 function¹³

$$U_{\text{exp-6}} = D_0 \left\{ \left[\left(\frac{6}{\gamma - 6} \right) e^{\gamma (1 - R/R_0)} \right] - \left[\left(\frac{\gamma}{\gamma - 6} \right) \left(\frac{R_0}{R} \right)^6 \right] \right\}$$
 (4)

Here R_0 is the equilibrium distance, D_0 is the equilibrium bond energy, and γ is a dimensionless quantity related to the force constant.

The last term in eq 1, U_{polar} , is the net polarization energy of the shell model, 14

$$U_{\text{polar}} = {}^{1}/_{2} \sum_{i} k_{i} \delta r_{i}^{2} \tag{5}$$

where the sum is over core—shell pairs. Here δr_i represents the displacement of the shell from the core. The shell model is included to account for the polarizabilities of Ag^+ and Br^- ions. In this simple approximation, the polarizable valence electrons are represented by a spherical shell connected to the core via a harmonic spring. The shell charge Q and the spring

^{*} To whom correspondence should be addressed.

[†] Present address: Department of Physics, MIT 13-3037, Cambridge, MA 02139.

[‡] Contribution No. 9127.

[⊗] Abstract published in Advance ACS Abstracts, September 1, 1995.

constant k are adjustable parameters, related to the (free-ion) polarizability by

$$\alpha_i = Q_i^2 / k_i \tag{6}$$

where α_i is an atomic polarizability. The shells are charged, and this electrostatic energy is included in the Coulomb sum, eq 2. Relativistic effects can be ignored since the shell velocity $v = \beta c$ leads to $\beta < 0.01$.

The convergence with distance of the sum in eq 1, especially the conditionally convergent Coulomb term, requires special attention. Since \mathbf{r}_i is the position within a unit cell and \mathbf{l} as the origin of that particular unit cell, the absolute position of atom i is $\mathbf{r}_i + \mathbf{l}$. The Coulomb potential and the London dispersion energy were evaluated with the Ewald method.¹⁵ The Coulomb sum is

$$S_{\text{Coulomb}} = \frac{1}{2} \lim_{L \to \infty} \sum_{i,j,l} \frac{q_i q_j}{r_{i,j,l}}$$

$$= \frac{1}{2} \sum_{i,j,l} \frac{q_i q_j}{q_i q_j} + \frac{1}{2\pi \Omega} \sum_{\mathbf{h} \neq 0} |F(\mathbf{h})|^2 \frac{e^{-b}}{h^2} - K \sum_{i,j,l} q_i^2 + \frac{1}{2\Omega} \int_{\partial V(L)} (\mathbf{d} \cdot \mathbf{r}) (\mathbf{d} \cdot \mathbf{n}) r^{-3} \, dS \quad (7)$$

where $a = \pi^{1/2}Kr_{i,j,l}$, $b = \pi h^2/K^2$, h is the reciprocal lattice vector, Ω is the unit cell volume $r_{i,j,l} = |\mathbf{r}_i - (\mathbf{r}_j + \mathbf{l})|$, and K is the Ewald parameter determining the relative size of the real space sum versus the reciprocal space sum. [See ref 15 or 16 for more details.] The last term in eq 7 is ignored because it is nonzero only for noncentrosymmetric crystal structures. (It represents a surface charge. 17) The unit cells are charge neutral.

The London dispersion energy sum is 15,17

$$S_{\text{London}} = \frac{1}{2} \sum_{i,j,l} \frac{C_{ij}}{r_{i,j,l}^{6}}$$

$$= \frac{1}{2} \sum_{i,j,l} \frac{q_{i}q_{j}}{r_{i,j,l}^{6}} (1 + a^{2} + a^{4}/2) e^{-a^{2}} + \frac{\pi^{9/2}}{3\Omega} \sum_{\mathbf{h} \neq 0} |F(\mathbf{h})|^{2} h^{3} \left[\pi^{1/2} \operatorname{erfc}(b) + \left(\frac{1}{2b^{3}} - \frac{1}{b} \right) e^{-b^{2}} \right] + \frac{\pi^{3} K^{3}}{6\Omega} (\sum_{i} q_{i})^{2} - \frac{1}{12} \pi^{3} K^{6} (\sum_{i} g_{i}^{2})^{2}$$
(8)

[See ref 15 or more details.] The prime indicates exclusion of the core—shell terms on same ion and of the i = j term for l = 0. The short-range repulsions are summed over all interactions within 8 Å. This ensures accuracy to within 0.01 kcal/mol.

We proceeded systematically to decouple the different parameters involved in the potentials. First, we examined a potential with just Coulomb and short-range terms (no polarization). Then we added shells to represent the Br⁻ ion polarizability, since it is greater than the Ag⁺ polarizability. Finally, shells were included with the Ag⁺ ions to more accurately model the crystal dielectric constant. The total potential sums all the interactions described above. For each model, parameters were fit to available experimental data at approximately 0 K (i.e.,

lattice constant, ¹⁸ phonon frequencies at Γ and X points of the Brillouin zone, ¹⁹ dielectric constant, ²⁰ lattice energy, ²¹ and elastic constants ¹⁹).

The Hessian (second-derivative matrix) **D** is defined as

$$D_{ia,jb} = \frac{\partial^2 U}{\partial r_{ia} \, \partial r_{jb}} \tag{9}$$

where r_{ia} is the a component (a, b = x, y, or z) of the *i*th center. The phonon modes were evaluated by assigning small finite masses (0.001 amu) to the shells and then diagonalizing the Hessian. The static dielectric tensor is calculated by^{22,23}

$$\epsilon_{0_{ab}} = \delta_{ab} + (4\pi/\Omega) \sum_{i,j} q_i q_j D_{ia,jb}^{-1}$$
 (10)

The high-frequency dielectric constants were calculated by^{22,23}

$$\omega_{\rm L}^2 = (\epsilon_0/\epsilon_{\infty})\omega_{\rm T}^2 \tag{11}$$

where ω_L and ω_T are the longitudinal and transverse optical-mode frequencies. Only the shell vibrations contribute to the high-frequency dielectric constant ϵ_{∞} . Literature data obey relation 11 only to within 10%, perhaps due to experimental uncertainty in the phonon frequencies.

We examined different shell charges and ionic charges. The absolute ionic charge determines the major part of the cohesive energy. The phonon curves can be fit by adjusting other parameters, such as shell charges and spring constants. We found that setting the ionic charge to q = 1 predicts the lattice energy reasonably well. Hence, we fixed the ionic charge at q = 1 so that the calculated lattice energy can be fit to the experimental cohesive energy. To reduce the number of parameters in the fitting procedures, we postulated different shell charges and then optimized the spring constants and short-range interactions. The best result has been found at $Q_{\rm Br}^- = -4.0$ for models with only the Br⁻ ion polarizable and $Q_{Ag^+} = -8.0$ and $Q_{\rm Br}^- = -5.0$ for models with both ions polarizable. Therefore, we set the shell charges at these values and varied only the spring constants and short-range interaction parameters when exploring different models.

The shell masses were originally treated as parameters. We found that different shell masses (within the order of an electron mass) had negligible effect on the various properties. Consequently, we set the shell mass to 0.001 amu.

III. Results

Figures 1-6 illustrate the fits of different models to the wave-vector-dependent phonon dispersion curves obtained by neutron scattering at 4.4 K.¹⁹

The parameters determined for the various models are tabulated in Table 1. Table 2 lists the properties calculated from the various models. We used either Lennard-Jones or Exp-6 potentials for both the one-shell model and the two-shell models. We found that Exp-6 does significantly better than Lennard-Jones for this system. The final parameters for the Exp-6 potential lead to an equilibrium distance R_0 between Ag^+ and Br^- of about 4.2 Å, whereas the Ag^+ - Br^- distance in the AgBr crystal is around 3 Å. That is, the ions are well into the repulsive part of the potential. The fits with the Lennard-Jones potential are of low quality, and these results are not shown. We therefore used the Exp-6 potential for all models. The parameters were optimized independently by fitting with the available experimental data by singular value decomposition method.²⁴

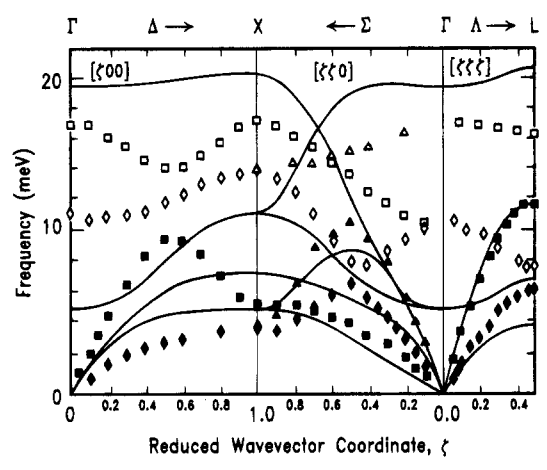


Figure 1. Phonon dispersion curves along the $[\xi,0,0]$, $[\xi,\xi,0]$, and $[\xi,\xi,\xi]$ directions in AgBr. The solid curves are from model I, and the symbols are experimental values (at 4.4 K, ref 19).

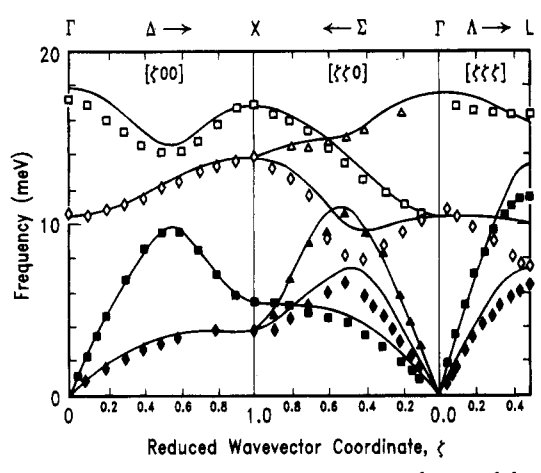


Figure 2. Phonon dispersion curves along the $[\xi,0,0]$, $[\xi,\xi,0]$, and $[\xi,\xi,\xi]$ directions. The solid curves are from model II, and the symbols are experimental values (at 4.4 K, ref 19).

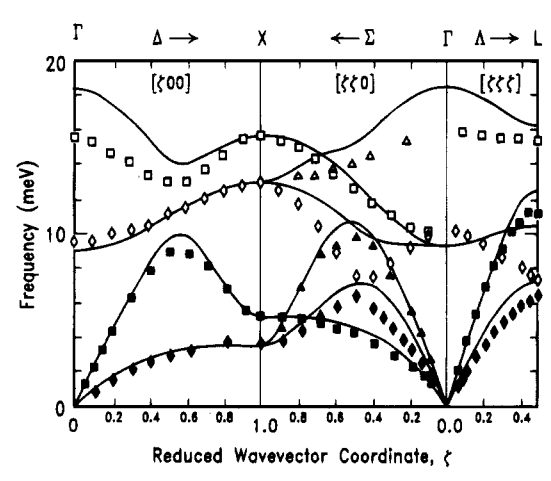


Figure 3. Phonon dispersion curves along the $[\xi,0,0]$, $[\xi,\xi,0]$, and $[\xi,\xi,\xi]$ directions. The solid curves are from model III, and the symbols are experimental values (at 4.4 K, ref 19).

Model I is a rigid ion model. The potential contains only Coulomb and Exp-6 interactions, with the ionic polarizabilities ignored. As noted in previous studies of AgCl²⁵ and AgBr,³ good agreement between computed and experimentally observed properties cannot be achieved without including polarization effects. Figure 1 shows the calculated and the experimental¹⁹ phonon dispersion curves. The phonon dispersion frequencies, especially the optical photons, are in poor agreement with the

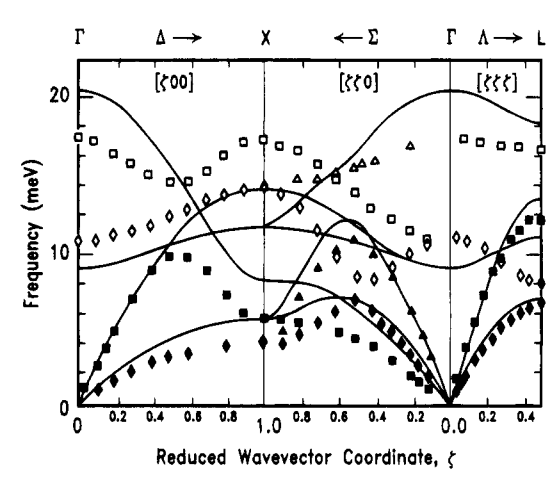


Figure 4. Phonon dispersion curves along the $[\xi,0,0]$, $[\xi,\xi,0]$, and $[\xi,\xi,\xi]$ directions. The solid curves are from model IV, and the symbols are experimental values (at 4.4 K, ref 19).

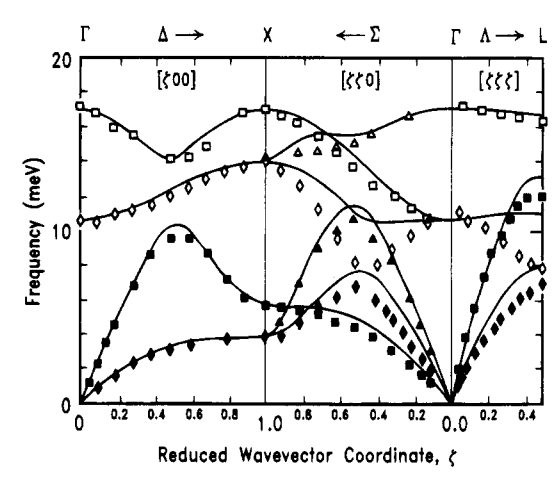


Figure 5. Phonon dispersion curves along the $[\xi,0,0]$, $[\xi,\xi,0]$, and $[\xi,\xi,\xi]$ directions. The solid curves are from model V, and the symbols are experimental values (at 4.4 K, ref 19).

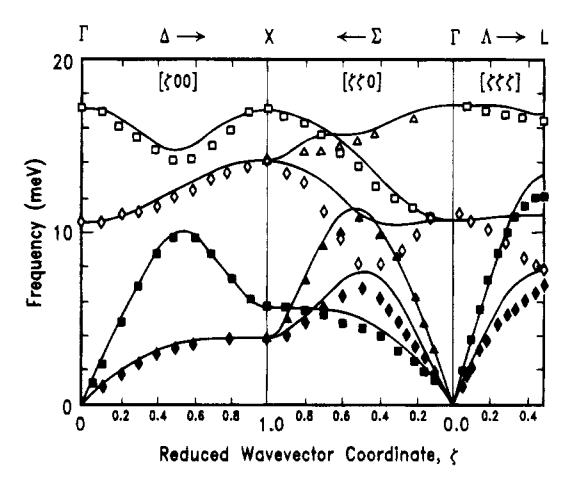


Figure 6. Phonon dispersion curves along the $[\xi,0,0]$, $[\xi,\xi,0]$, and $[\xi,\xi,\xi]$ directions. The solid curves are from model VI, and the symbols are experimental values (at 4.4 K, ref 19).

literature values. The lattice energy, listed in Table 2, is clearly too low, and the elastic constants are not reproduced with reasonable accuracy.

Model II assumes that only the Br⁻ ion is polarizable. Early work on AgBr lattice dynamics^{3,12} demonstrated that a reasonable fit can be obtain with shells on the more polarizable Br⁻ ion. Figure 2 shows the calculated and experimental phonon dispersion curves. Model II contains Exp-6 interactions for Ag⁺

TABLE 1: Potential Parameters for AgBra

			model				
			ř.			37	
			ĪI	III_	IV	V	VI
	_	,	,	Paramete	ers ^b		
Ag_c-Ag_c	R_0	3.179	0.915	2.908			3.293
	D_0	0.192	0.143	0.159			0.172
	γ	12.411	6.694	11.865			11.878
Br_c-Br_c	R_0	6.836		3.734			3.858
	D_0	0.023		11.034			4.088
	γ	13.233		15.215	• • • •		18.468
Ag_s-Ag_s	R_0				2.961		
	D_0				0.124		
	γ				12.950		
Br_s-Br_s	R_0				3.739		
	D_0				7.259		
	γ				10.205		
Ag_s-Ag_c	R_0					3.228	
	D_0					0.175	
	γ					12.053	
Br_s-Br_c	R_0		3.829			3.831	
	D_0		2.292			3.165	
	γ		9.900			9.495	
Ag_s-Br_c	R_0					4.162	4.078
	D_0					0.385	0.356
	γ					7.962	7.778
$Br_s - Ag_c$	R_0		4.217			4.309	4.093
	D_0		0.604			0.405	0.377
	γ		9.960			10.997	11.291
Ag_c-Br_c	R_0	3.000		6.072			3.836
_	D_0	0.525		0.035			0.359
	γ	20.198		12.125			8.653
Ag_s-Br_s	\dot{R}_0				5.590		3.932
U. ·	D_0				0.036		0.365
	γ				12.280		9.026
(b) Variable Shell Parameters							
I.		(U) V	arrable .	24742	57948	11951	18427
k_{Ag}			1257	4555	2409	2001	1931
k_{Br}						2001	1931
(c) Fixed Shell Parameters							
Q_{Ag}				8.0	8.0	8.0	8.0
Q_{Br}			4.0	5.0	5.0	5.0	5.0

^a See eqs 3, 4, and 6 for definitions. R_0 is in units of Å, D_0 is in unit of kcal/mol, γ is dimensionless, the spring constant k is in kcal/(mol Å²), and the charge Q is in au. ^b The subscript c and s indicate the core and the shell, respectively. The shell charges are fixed parameters.

core—Ag⁺ core, Br⁻ core—Br⁻ shell, and Ag⁺ core—Br⁻ shell. The calculated phonon dispersion curves are in excellent agreement with experimental values with only Br⁻ polarizable.

The calculated static dielectric constant is lower than the literature data. This is expected since the polarizability is also predicted to be too low. The static dielectric ϵ_0 is related to the crystal polarizability by eq 10, ore more symbolically by

$$\epsilon_0 = 1 + (4\pi/\Omega)\alpha^{\text{crystal}} \tag{12}$$

The crystal polarizability $\alpha^{crystal}$ is approximately the sum of the atomic polarizabilities and the displacement polarizability 14

$$\alpha^{\text{crystal}} = (\alpha^+ + \alpha^-) + \alpha^{\text{dis}}$$
 (13)

Here α^+ is the atomic polarizability of the positive ion, α^- is the atomic polarizability of the negative ion, and α^{dis} is the displacement polarizability. From (13), we do not expect the dielectric constant to be accurately predicted, since the Ag^+ ion polarizability was not included. Table 2 confirms this expectation

Models III—VI contain a Ag⁺ shell as well as a Br⁻ shell. In model III, only the Coulomb interaction and the core—core Exp-6 are included. Model IV replaces the core—core Exp-6 term in model III with shell—shell Exp-6 interactions. In model

TABLE 2: Predicted Elastic and Optical Constants of AgBr at 0 K

	model							
	I	II	III	IV	V	VI	expt	
	(a) Phonons (cm ⁻¹) ^a							
$\Gamma_{ extsf{TO}}$	43.6	85.4	79.8	76.5	86.1	85.5	86.1	
$\Gamma_{ extsf{LO}}$	150.7	138.7	163.1	149.4	138.8	139.0	138.8	
X_{TA}	43.0	31.5	31.7	31.6	31.2	31.4	31.1	
X_{LA}	62.3	44.7	45.0	42.8	45.6	45.3	45.6	
X_{TO}	92.5	113.7	114.1	106.8	114.0	114.4	114.0	
X_{LO}	164.8	144.8	138.1	130.4	138.5	137.9	138.5	
rms^b	22.3	1.4	5.6	6.3	0.0	0.4		
	(b) Dielectric Constant							
ϵ_0	12.96	7.63	8.09	10.42	10.60	9.58	10.60	
ϵ_{∞}	1.08	2.89	1.94	2.73	4.08	3.62	4.68	
	(c) Elastic Constant (GPa)							
C_{11}	34.1	63.7	81.6	66.7	72.1	73.0	71.2	
C_{12}	29.2	11.9	12.2	13.0	11.3	11.2	35.5	
C_{44}	30.1	11.9	12.2	13.0	11.3	11.2	8.5	
(d) Cohesive Energy (eV)								
U	8.12	8.90	8.58	8.42	9.34	9.01	9.33	

 a The phonons were fit to the Γ and X points. b rms is the root-mean-square deviation of frequencies.

TABLE 3: Electronic Polarizabilities of Ions (in Å³)

ion	TKS ³⁰	WC ³¹	DBV ³	GDM ³²	MB ³³	model V
Ag ⁺	2.4	* **	2.00	2.00	1.67	1.72
Br ⁻	4.16	4.023-4.606	5.03	4.28	4.55	4.02

TABLE 4: Comparison of Model Potentials

	no. of	shell					
model	parameters	Ag	Br	vdw	characteristics		
I	9	no	no	exp-6	rigid ion (all core-core)		
II	10	no	yes	exp-6	Ag_c-A_c , Ag_c-Br_s , Br_c-Br_s		
III	11	yes	yes	exp-6	all core-core, none involving shells		
IV	11	yes	yes	exp-6	all shell—shell, none involving core		
V	11	yes	yes	exp-6	all core—shell, none involving core—core or shell—shell		
VI	17	yes	yes	ехр-б	all core-core plus all Ag-Br		

V, there are only core—shell interactions. Model VI contains core—core Exp-6 for like ions (Ag⁺—Ag⁺ and Br⁻—Br⁻) and core—core, shell—shell, and shell—core Exp-6 for different ions (Ag⁺—Br⁻). The calculated phonon dispersion curves for model III (with Exp-6 on cores only) and models IV, V, and VI (with exp-6 on shells only) are shown in Figures 3—6. We found that model V provides the best fit among the various models (Table 2, Figure 5). These characteristics of the various potential are summarized in Table 4.

Model II contains the fewest adjustable parameters among the various models and predicts phonon dispersion curves reasonably well. The one-phonon density of states calculated for model II at 0 K is shown in Figure 7. The distributions are similar to those obtained from lattice dynamics.³ The calculated specific heat versus temperature for model II is shown in Figure 8.

IV. Discussion

These interaction potentials produced phonon dispersion curves in excellent agreement with the experimental data, especially the anomalous optical phonon curves unique to AgBr crystal. They also exhibit the characteristic inversion of the TA and TO modes in the phonon dispersion curves at the L point. The calculated dielectric constant and the lattice energy are also in accord with the measured values. The excellent

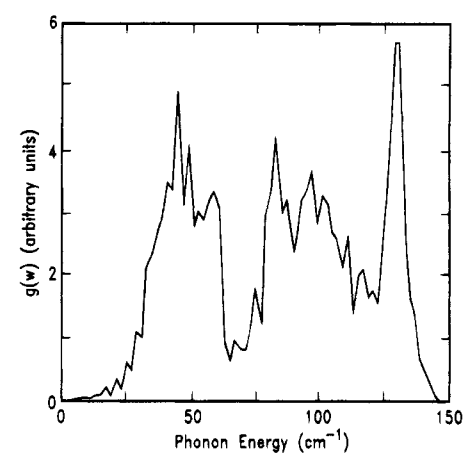


Figure 7. One-phonon density of states at 0 K calculated for model

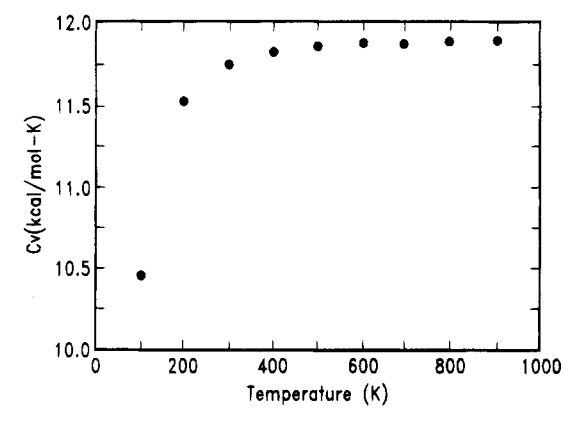


Figure 8. Specific heat versus temperature calculated for model II.

agreement with the experimental data suggests that a pairwise potential can be applied with some confidence to the simulation of crystal properties. Indeed, the shell model has played an important role in modeling polarization effects in ionic systems. While the shell model has not been considered applicable to molecular dynamics simulations, ²⁶ the development of a new theoretical approach²⁷ to deal with shell motions may render the shell model usable in dynamical simulations.

The elastic constant C_{12} was not fit because the strong Cauchy violation cannot be simulated by a simple pairwise potential. A proper description requires either bonding terms or manybody potentials such as three-body van der Waals interactions. However, a macroscopic parameter such as C_{12} should have little effect on microscopic details such as defect energies and ionic diffusion coefficients.

Practical calculations of the properties for AgBr crystal have focused on point defects because of their relevance to the photographic processes. For example, defect formation enthalpy and entropy as well as diffusion have been studied. The bond angle bending terms introduced by Baetzold *et al.*¹⁰ provide an accurate description of the modes. However, it is not clear how to use such an approach for calculation of defect properties, since a consistent treatment of the *absence* in bonding at defect sites is not apparent. Therefore, we restricted our potential to a simple pairwise form to represent the characteristic properties of AgBr crystal.

Strikingly, model II (only Br⁻ ion polarizable) predicts phonon dispersion curves that are essentially identical to those from the model with both ions polarizable. This indicates that the strong van der Waal forces and the high Br⁻ polarizability are responsible for the phonon dispersion curves unique to AgBr crystals. This outcome is consistent with the single-crystal

X-ray diffraction data on the electron density distribution map. 28 The radial distribution function of the bromine 4p electrons in the crystal differs far more from the free ion state than does the radial distribution function of the silver 4d electrons. Therefore, we conclude that the distinctive properties of silver halides result from deformation of the outmost p electrons of halogen ion and not the deformation of silver ions.

In our simulations, the shell mass is set to approximately an electron mass (0.001 amu). We examined the effect of the shell mass by increasing it by a factor of 100 (to 0.1 amu). This led to minimal changes in physical properties. (For example, the phonon frequencies shift by less than 1 cm⁻¹.) This result is expected due to the disparate frequencies of shell and core vibrations. Our present treatment of the shell model differs from the commonly adopted shell model by Dick and Overhauser,²⁹ in that there is a nonzero shell mass. The classical treatment of shell motions ignores the zero-point motions. The magnitude of the zero-point energy of the cores are on the order of 0.1 eV, which is negligible compared to the lattice energy. On the other hand, the electron shell zero-point motions are about 5-10eV, which is comparable to the lattice energy. Consequently, this quantum effect should be incorporated to fully illustrate the lattice dynamics. The assignment of a finite mass to the shell is important since it leads to an approximately correct quantum mechanical treatment of the shell model. A more detailed treatment of the shell model is presented in ref 27.

Model V gave the best fit among these models. The model contains shell-core Exp-6 interactions and also contains Coulomb interactions and harmonic springs. Model VI, though containing more adjustable parameters, does not improve the simulation of crystal properties over model V. Model V successfully predicts the overall trend of the phonon dispersion curves as well as the inversion of TA and TO phonon modes at L point without introducing any term to account for the quadrupolar deformation of Ag⁺ ion. The phonon modes at the Γ and X points, the static dielectric constant ϵ_0 , and the cohesive energy were fit to within 0.1% of the literature data (Table 2). The atomic polarizabilities obtained by this model are $\alpha_{Ag^+} = 1.72 \text{ Å}^3$ and $\alpha_{Br^-} = 4.02 \text{ Å}^3$. As illustrated in Table 3, the atomic polarizabilities determined by this model are plausible when compared to values determined by different $methods.^{2,30-33}$

V. Comparison with Other Models

The interaction potentials obtained by Bucher¹¹ and Baetzold *et al.*¹⁰ contain three-body terms to take into account the Cauchy violation but were unable to predict the phonon dispersion curves. In ref 10, the phonon dispersion curves (especially the optical phonons), calculated using 17 parameters, are in poor agreement with experimental data. The authors concluded that quadrupolar deformation of the Ag⁺ was needed to produce the optical phonon modes. However, we have found a simple pairwise potential that simulates most of the crystal properties (e.g., dielectric constant and phonon dispersion curves). This indicates that the strong van der Waals interactions and the polarization effects are important in understanding the phonon dispersion curves unique to AgBr crystal. Since the potential contains only two-body interactions and does not have bonding terms, it can be applied easily to simulations of defect properties.

VI. Conclusion

We have produced a pairwise potential for AgBr, which predicts properties in agreement with experiment. We found that Br⁻ polarizability and van der Waals interactions are important for the AgBr crystal. This shell model provides a

useful tool for examining polarization effects on the crystal properties (for both phonon dispersion frequencies and dielectric effects) and should be useful for calculating properties involving defects.

Acknowledgment. We thank Dr. Naoki Karasawa for helpful discussions and Molecular Simulations Inc. for use of POLYGRAF.^{34,35} The research was funded by the NSF (CHE 91-100289, CHE 94-13930, and ASC 92-100368). The facilities of the MSC are also supported by grants from DOE-BCTR, Allied-Signal Corp., Aramco, Asahi Chemical, Asahi Glass, BP Chemical, Chevron Petroleum Technology, Oronite, BF Goodrich, Xerox, Vestar, Hercules, Hughes Research Lab., and Beckman Institute. Some calculations were carried out at the NSF Supercomputer Centers (Pittsburgh and San Diego) and on the JPL Cray.

References and Notes

- (1) Hamilton, J. F. Adv. Phys. 1988, 37, 359.
- (2) von der Osten, W. The Physics of Latent Image Formation in Silver Halides; International Symposium, Trieste; Baldereschi, A., Czaja, W., Tosatti, E., Tosi, M., Ed.; World Scientific: Singapore, 1983; p. 1.
- (3) Dorner, B.; von der Osten, W.; Bührer, W. J. Phys. C 1976, 9, 723.
 - (4) Bührer, W. Phys. Status Solidi B 1975, 68, 739.
 - (5) Friauf, R. J. J. Phys. (Paris) 1987, 20, 705.
 - (6) Devlin, B. A.; Corish, J. J. Phys. C 1987, 20, 705.
- (7) Cowley, R. A.; Cochran, W.; Brockhouse, B. N.; Woods, A. D. B. *Phys. Rev.* **1963**, *131*, 1030.
 - (8) Slifkin, L. Philos, mag. A 1991, 64, 1035.
 - (9) Mayer, J. E. J. Chem. Phys. 1933, 1, 327.
- (10) Baetzold, R. C.; Catlow, C. R. A.; Corish, J.; Healy, F. M.; Jacobs, P. W. M.; Leslie, M.; Tan, Y. T. J. Phys. Chem. Solids 1989, 50, 791.
 - (11) Bucher, M. Phys. Rev. B 1984, 30, 947.
- (12) Fischer, K.; Bilz, H.; Haberkorn, R.; Weber, W. Phys. Status Solidi 1972, 54, 285.

- (13) Mayo, S. L.; Olafson, B. O.; Goddard III, W. A. J. Phys. Chem. 1990, 94, 8897.
- (14) Ashcroft, N. W.; Mermin, N. D. Solid Static Physics; W. B. Saunders: Philadelphia, 1976; Chapter 27.
 - (15) Karasawa, N.; Goddard III, W. A. J. Phys. Chem. 1989, 93, 7320.
 - (16) Williams, D. E. Acta Crystallogr. A 1971, 27, 452.
- (17) Deem, M. W.; Newsam, J. M.; Sinha, S. K. J. Phys. Chem. 1990, 94, 8356.
 - (18) Lawn, B. R. Acta Crystallogr. 1963, 16, 1163.
- (19) Fujii, Y.; Hoshino, S.; Sakuragi, S.; Kanzaki, H.; Lynn, J. W.; Shirane, G. Phys. Rev. B 1977, 15, 358.
- (20) Lowndes, R. P.; Martin, D. H. Proc. R. Soc. London, A 1969, 308, 473
 - (21) Thurmond, C. D. J. Am. Chem. Soc. 1953, 75, 3929.
- (22) Born, M.; Huang, K. Dynamical Theory of Crystal Lattices; Oxford University Press: Oxford, 1954.
 - (23) Karasawa, N.; Goddard III, W. A. Macromolecules 1992, 25, 7268.
- (24) Yamasaki, T.; Dasgupta, S.; Goddard III, W. A. Hessian Biased Force Fields: II. The Singular Value Decomposition Based Least Squares Method for Optimization and Analysis of Force Field Parameters. *J. Chem. Phys.*, submitted for publication.
- (25) Vijayaraghavan, P. R.; Nicklow, R. M.; Smith, H. G.; Wilkinson, M. K. Phys. Rev. B 1970, 1, 4819.
- (26) Moscinski, J.; Jacobs, P. W. M. Proc. R. Soc. London A 1985, 398, 141-171.
 - 41–171. (27) Kiang, C.-H.; Goddard III, W. A. *J. Chem. Phys.* **1993**, 98, 1451.
- (28) Takahashi, H.; Tamaki, S.; Sato, S. J. Phys. Soc. Jpn. 1987, 56, 3583.
 - (29) Dick, B. G.; Overhauser, A. W. Phys. Rev. 1958, 112, 90.
- (30) Tessman, J. R.; Kahn, A. H.; Shockley, W. Phys. Rev. 1953, 15, 890.
 - (31) Wilson, J. N.; Curtis, R. M. J. Chem. Phys. 1970, 74, 187.
 - (32) Mahan, G. D. Solid State Ionics 1980, 1, 29.
 - (33) Bucher, M. Solid State Ionics 1984, 14, 7.
- (34) Calculations were carried out with POLYGRAF from Molecular Simulations Inc. (Burlington, MA) modified to include the shell model²³ and phonons.³⁵ This version is denoted V4.0.
- (35) Karasawa, N.; Dasgupta, S.; Goddard III, W. A. J. Phys. Chem. 1991, 95, 2260.

JP951054B